Journal of Statistical Physics, Vol. 48, Nos. 5/6, 1987

Mechanism and Nonlinear Dynamics of an Oscillating Chemical Reaction

A. M. Zhabotinsky[1] and A. B. Rovinsky[1]

Received February 11, 1987

A mechanism and a model of a ferroin-catalyzed oscillating chemical system are descrined. This reaction presents an excellent example of a far-from-equilibrium system that forms spatial and temporal dissipative structures. The model shows that while the well-stirred system has a unique and stable stationary state, the same reagent spread in a thin layer may form complex spatiotemporal paterns. Stationary periodic patterns of both small and large amplitude, standing waves, and inhomogeneous chaotic oscillations are found in the model.

KEY WORDS: Belousov–Zhabotinsky system; chemical oscillations; dissipative structures; diffusion instabilities; chaos.

1. INTRODUCTION

The history of the discovery and investigation of chemical oscillations is closely connected with the name of I. Prigogine. He found the thermodynamic conditions necessary chemical oscillations to arise.[1,2] Then he developed a general concept of self-organization in far-from-equilibrium systems and suggested the term "dissipative structures," which is commonly accepted now as implying nonequilibrium structures of different nature. A number of models of self-organization were studied by him and the Brussels school. The Brusselator is the best known among these models and it has been very helpful in the general theoretical analysis of chemical oscillators.

The reactions discovered by Belousov and initially studied by Zhabotinsky (BZ reaction) played a key role in experimentally proving that chemical oscillations really exist and show a great variety of dynamic regimes.[3,4]

[1] Institute of Biological Physics of the Academy of Science, Puschino, Moscow Region 142292, USSR.

0022-4715/87/0900-0959$05.00/0

Self-sustained traveling concentration waves present one of the most interesting phenomena discovered in the BZ reaction.[5,7] The chemical autowaves are usually studied in a BZ system catalyzed by $Fe(phen)_3^{2+}$ ion (ferroin). However, experimental investigations of well-stirred systems have been mostly carried out in cerium-catalyzed reactions, either because of historic reasons or a belief that the cerium-catalized system is simpler.

The FKN scheme[8] is commonly accepted as an adequate mechanism of the BZ reaction. However, the Oregonator model derived from an oversimplified version of the FKN scheme shows significant quantitative discrepancies with the experimental data obtained in the system catalyzed by the cerium ion.[9 12]

A mathematical model of the bromate–ferroin–bromomalonic acid system has been developed recently on the basis of the FKN scheme for analysis of spatial phenomena.[13] This model appears to describe quantitatively well oscillations and waves studied in the experiment.[14]

One of the interesting problems in this field is to find experimentally the stationary periodic structures predicted by Turing.[15] Small-amplitude Turing patterns have been theoretically investigated in more detail than any other dissipative structure is reaction-diffusion systems. However, there has been no clear evidence that these structures have been observed in experiments with chemical systems. Our knowledge of the behavior of large-amplitude stationary patterns is also very limited.

This paper presents a model of the ferroin-catalyzed BZ reaction and the analysis of small- and large-amplitude stationary periodic structures as well as standing waves and chaotic inhomogeneous oscillations arising in this model due to diffusion instabilities.

2. MECHANISM AND MODEL OF THE BROMATE–FERROIN–BROMOMALONIC ACID REACTION

The chemical mechanism underlying the oscillations and excitability of the system is assumed to be accounted for by the skeleton scheme[2 5]

$$H^+ + HBrO_2 + HBrO_3 \rightleftharpoons HBrO_2^+ + BrO_2^{\cdot} + H_2O \quad (1)$$

$$BrO_2^{\cdot} + H^+ \rightleftharpoons HBrO_2^+ \quad (2)$$

$$Me^{n+} + HBrO_2^+ \rightleftharpoons Me^{(n+1)+} + HBrO_2 \quad (3)$$

$$2HBrO_2 \rightleftharpoons HOBr + HBrO_3 \quad (4)$$

$$H^+ + Br^- + HBrO_2 \rightleftharpoons 2HOBr \quad (5)$$

$$H^+ + Br^- + HOBr \rightleftharpoons Br_2 + H_2O \quad (6)$$

$$H^+ + Br^- + HBrO_3 \rightleftharpoons HBrO_2 + HOBr \tag{7}$$

$$Me^{(n+1)+} + CHBr(COOH)_2 \rightleftharpoons Me^{n+} + H^+ + {}^{\cdot}CBr(COOH)_2 \tag{8}$$

$$H_2O + {}^{\cdot}CBr(COOH)_2 \rightleftharpoons H^+ + Br^- + {}^{\cdot}COH(COOH)_2 \tag{9}$$

$$HOBr + CHBr(COOH)_2 \rightleftharpoons CBr_2(COOH)_2 + H_2O \tag{10}$$

$$Br_2 + CHBr(COOH)_2 \rightleftharpoons CBr_2(COOH)_2 + H^+ + Br^- \tag{11}$$

$$H_2O + CHBr(COOH)_2 \rightleftharpoons CHOH(COOH)_2 + H^+ + Br^- \tag{12}$$

$${}^{\cdot}COH(COOH)_2 + CHBr(COOH)_2 \rightleftharpoons CHOH(COOH)_2 + {}^{\cdot}CBr(COOH) \tag{13}$$

$$Me^{(n+1)+} + {}^{\cdot}COH(COOH)_2 \rightleftharpoons CO(COOH)_2 + Me^{n+} + H^+ \tag{14}$$

$$CO(COOH)_2 \rightleftharpoons OCHCOOH + CO_2 \tag{15}$$

The ferroin and cerium catalysts differ mainly in the value of the redox potential: for the $Fe(phen)_3^{2+}/Fe(phen)_3^{3+}$ couple it equals 1.14 V and for the couple Ce^{3+}/Ce^{4+} it is 1.61 V. Therefore, in the cerium case the reverse reaction (3) is very significant, while reaction (8) can be regarded as irreversible and vice versa for the ferroin case.[9,10,17] Scheme (1)–(15) does not provide a quantitative description of experimental results for the reaction catalyzed by cerium.[13] For the ferroin-catalyzed reaction the system of differential equations

$$\begin{aligned}
\dot{X} &= k_3 U(C-Z) - k_{-3} XZ - k_1 h_0 AX + k_{-1} U^2 - 2k_4 h_0 X^2 \\
&\quad - k_5 h_0 XY + k_7 h_0 AY \\
\dot{Y} &= qk_9 R - k_7 h_0 AY - k_5 h_0 XY \\
\dot{Z} &= k_3 U(C-Z) - k_{-3} XZ - k_8 BZ + k_{-8} h_0 R(C-Z) \\
\dot{U} &= k_3 U(C-Z) + k_{-3} XZ + 2k_1 h_0 AX - 2k_{-1} U^2 \\
\dot{R} &= k_8 BZ - k_{-8} h_0 (C-Z) R - k_9 R
\end{aligned}$$

(where $X = [HBrO_2]$, $Y = [Br^-]$, $Z = [Fe(phen)_3^{3+}]$, $U = [HBrO_2^+]$, $R = [{}^{\cdot}CBr(COOH)_2]$, $A = [HBrO_3]$, $B = [CHBr(COOH)_2]$, $C = [Fe(phen)_3^{2+}] + [Fe(phen)_3^{3+}]$, and h_0 is the acidity function) corresponding to steps (1)–(15) can be reduced to a two-variable system with methods of singular perturbation theory. The variables of this reduced system are $HBrO_2$ and $Fe(phen)_3^{3+}$. In scaled form the equations are

$$\begin{aligned}
\varepsilon \frac{dx}{d\tau} &= x(1-x) - \left(2q\alpha \frac{z}{\varepsilon' + (1-z)} + \beta \right) \frac{x-\mu}{x+\mu} = f(x, z) \\
\frac{dz}{d\tau} &= x - \alpha \frac{z}{\varepsilon' + (1-z)} = g(x, z)
\end{aligned} \tag{16}$$

where

$$X=\frac{k_1 A}{2k_4}x, \qquad Z=Cz, \qquad t=\frac{k_4 C}{k_1^2 A^2 h_0}\tau$$

$$\alpha=\frac{k_4 k_8 k_9 B}{k_{-8}k_1^2 A^2 h_0^2}, \qquad \beta=\frac{k_4 k_{12} B}{k_1^2 A^2 h_0}, \qquad \mu=\frac{2k_4 k_7}{k_1 k_5}$$

$$\varepsilon=\frac{k_1 A}{k_4 C}, \qquad \varepsilon'=\frac{k_9}{k_{-8}Ch_0}$$

q is a stoichiometric factor. Almost always the term ε' can be neglected. Analysis of kinetic and thermodynamic experimental data provides the following set of rate constants[13]:

$$k_1 = 100\ \mathrm{M}^{-2}\,\mathrm{sec}^{-1}, \qquad k_4 = 1.7\times 10^4\ \mathrm{M}^{-2}\,\mathrm{sec}^{-1}, \qquad k_5 = 10^7\ \mathrm{M}^{-2}\,\mathrm{sec}^{-1}$$

$$\frac{k_8 k_9}{k_{-8}} = 2\times 10^{-5}\ \mathrm{M\,sec}^{-1}, \qquad k_{12} = 1\times 10^{-6}\ \mathrm{sec}^{-1}, \qquad q = 0.5$$

These values agree with other estimates.[12,18–20] Model (16) is in good quantitative agreement with the experiments in a well-stirred reactor (Fig. 1).

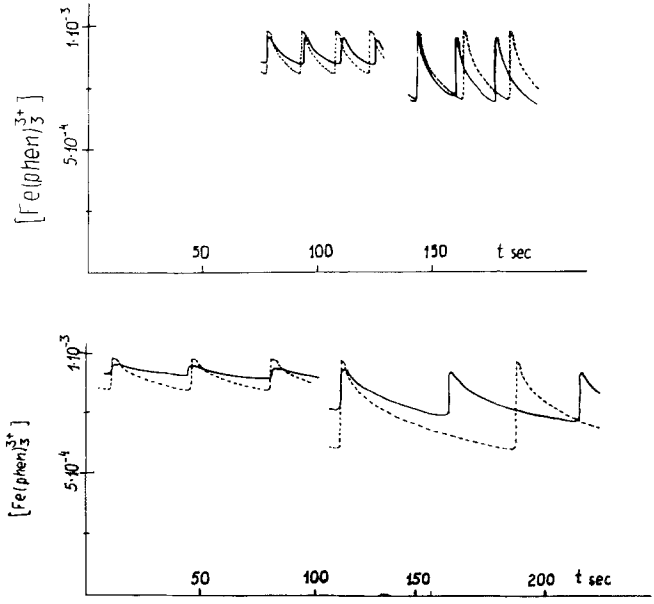

Fig. 1. Oscillations in the bromate–ferroin–bromomalonic acid system. (——) Experiment; (- -) the model. (Top) $A=0.05$, $B=0.2$, $C=0.001$, and $h=2.1$, and $A=0.05$, $B=0.37$, $C=0.001$, $h_0=2.1$; (bottom) $A=0.025$, $B=0.2$, $C=0.01$, and $h=2.5$, and $A=0.025$, $B=0.4$, $C=0.001$, and $h_0=2.5$.

3. DISSIPATIVE STRUCTURES IN THE MODEL OF THE FERROIN OSCILLATOR

Adding diffusion terms to model (16) produces the reaction-diffusion system

$$\begin{aligned} x_\tau &= (1/\varepsilon) f(x, z) + \Delta x \\ z_\tau &= g(x, z) + \kappa \Delta z \end{aligned} \tag{17}$$

where

$$\kappa = D_Z/D_X, \qquad r_i = (k_4 C D_X/k_1^2 A^2 h_0)^{1/2} \rho_i$$

($i = 1, 2, 3$; r_i are spatial coordinates, ρ_i are scaled spatial coordinates).

For $\kappa = 1$, model (16), (17) describes quite well spatial structures formed by traveling waves (e.g., by single and multiarmed spiral waves) (Fig. 2).[14]

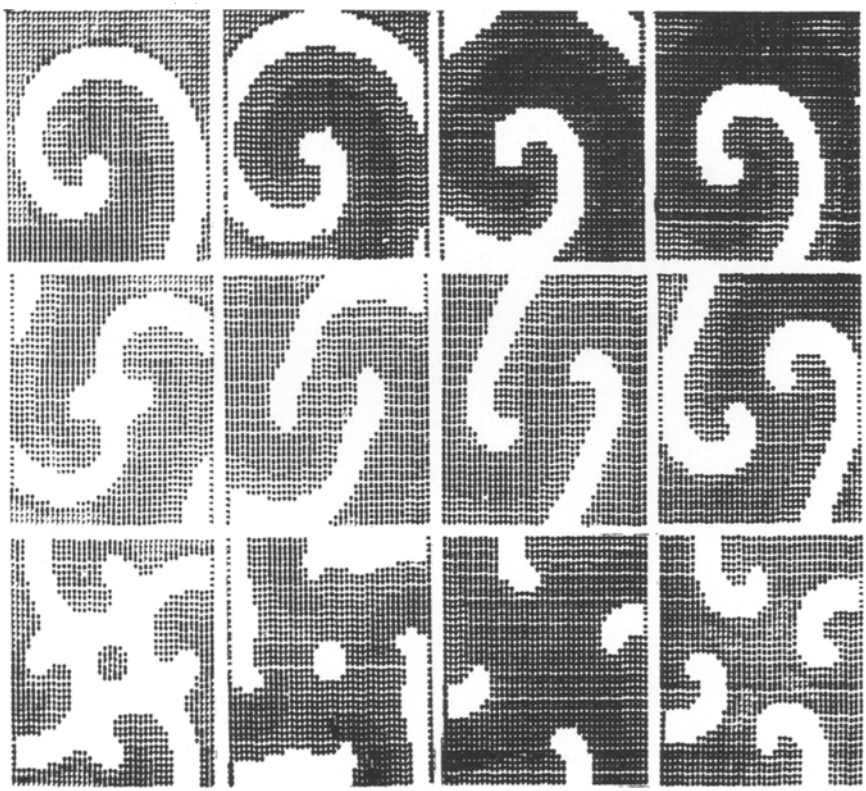

Fig. 2. Evolution of the cores of the single-, two-, and four-armed spirals in model (17). Time interval between the consecutive positions is 1.45 sec. $A = 0.03$, $B = 0.3$, $C = 0.001$, $h_0 = 2$.

Now it is interesting to seek the structures arising due to diffusion instablity of the homogeneous stationary state. For this purpose we should find the conditions under which system (16) is stable while system (17) is not. These are

$$\text{(a)} \quad \frac{1}{\varepsilon}\frac{\partial f}{\partial x}+\frac{\partial g}{\partial z}<0$$

$$\text{(b)} \quad \frac{\kappa}{\varepsilon}\frac{\partial f}{\partial x}+\frac{\partial g}{\partial z}>0$$

Since $\partial g/\partial z$ is always negative, the Turing bifurcation is only possible for $\kappa > 1$ and $\partial f/\partial x > 0$. Values of the diffusion coefficients of $HBrO_2$ and $Fe(phen)_3^{3+}$ are not available, but since ferroin is a charged ion with a higher molecular weight than that of bromous acid, one may expect that the diffusibility of bromous acid exceeds that of ferroin, which means that

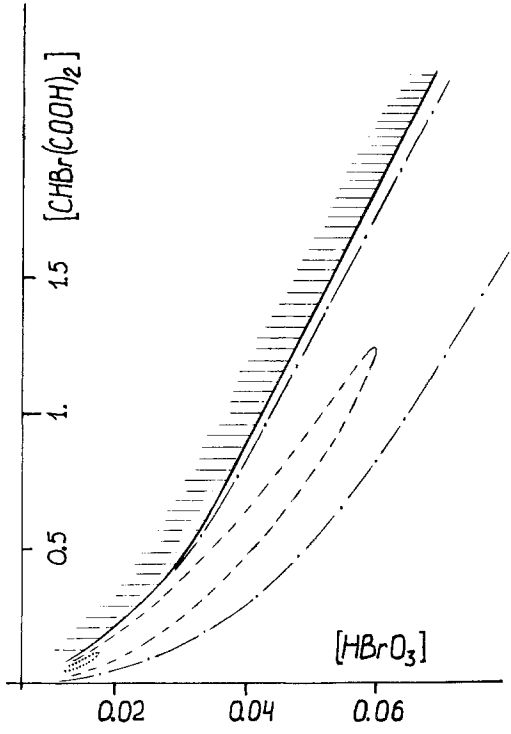

Fig. 3. Domains of linear stability, bulk oscillations, and aperiodic instability in model (17). (Details in the text). (···) $C = 3 \times 10^{-6}$, (- -) $C = 10^{-5}$, (-·-) $C = 3 \times 10^{-5}$.

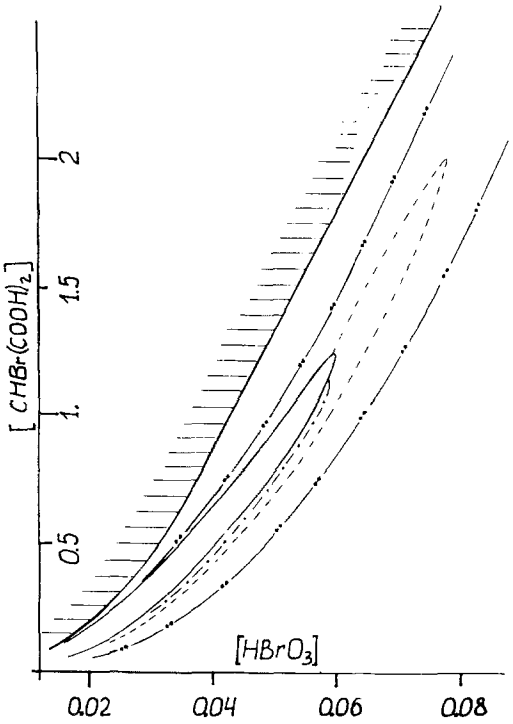

Fig. 4. Domains of Turing instability in the (A, B) plane for different values of the ratio $\kappa = D_Z/D_X$. (---) $\kappa = 1.5$, (- -) $\kappa = 2$, (-·-·-) $\kappa = 4$.

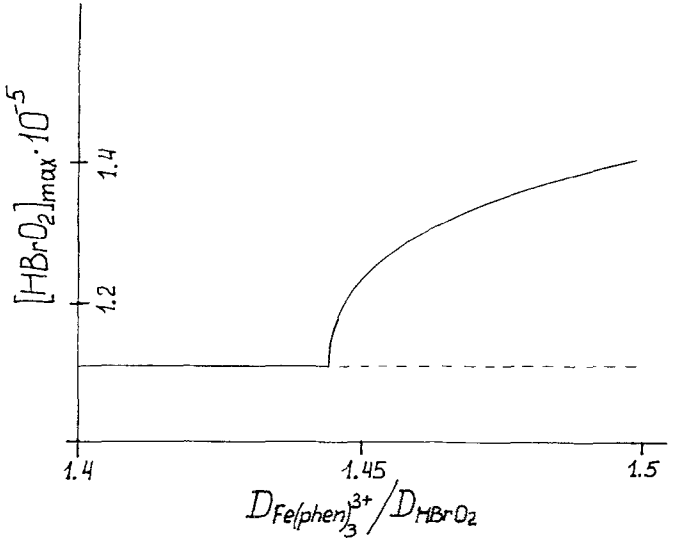

Fig. 5. Stationary state diagram for $A = 0.044$, $B = 0.57$, $C = 10^{-5}$, $h_0 = 1$.

$\kappa < 1$. If so, Turing bifurcation is impossible under normal conditions. Nevertheless, it is interesting to analyze the effect of κ on the spatial behavior of model (17).

Figure 3 shows how the total catalyst concentration affects the boundary of linear stability of the system (17) on the (A, B) plane. In the shaded region the homogeneous steady state of the system is always linearly stable [the boundary of the region is the line $(\partial f/\partial x)\,\partial g/\partial z - (\partial f/\partial z)\,\partial g/\partial x = 0$]. Its position does not depend on C. The lines of Hopf bifurcation are given for three values of C. They limit the domains of bulk oscillations. In the area beyond the shaded region and the bulk oscillation region the Turing bifurcation can occur and this area gets large with decreasing C. Figure 4

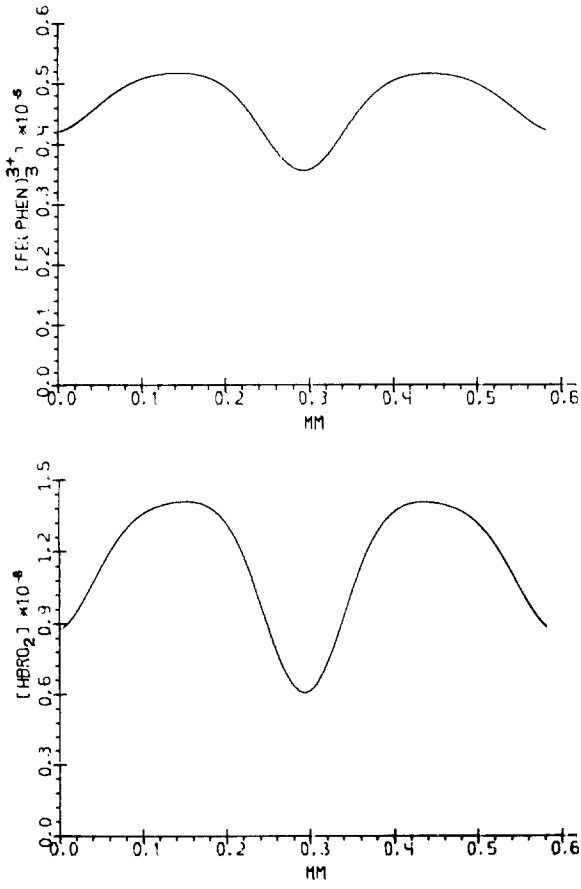

Fig. 6. A small-amplitude stationary pattern for $\kappa = 1.5$. Other conditions as for Fig. 5.

shows the influence of the parameter κ on the position of the line of the Turing bifurcation on the plane (A, B). The area of instability of the homogeneous state expands with increase of κ.

In what follows we consider a one-dimensional limited system with Neumann boundary conditions (impenetrable walls). The results are obtained either by direct integration of system (17) or numerical investigation of its stationary solutions (found with the Newton technique) and their stability.

A stationary state diagram for the small-amplitude Turing structure is presented in Fig. 5 and the corresponding stationary pattern is shown in Fig. 6. In many cases, however, a large-amplitude pattern arises as a result of small perturbations of an initially homogeneous state (Fig. 7). Figure 8

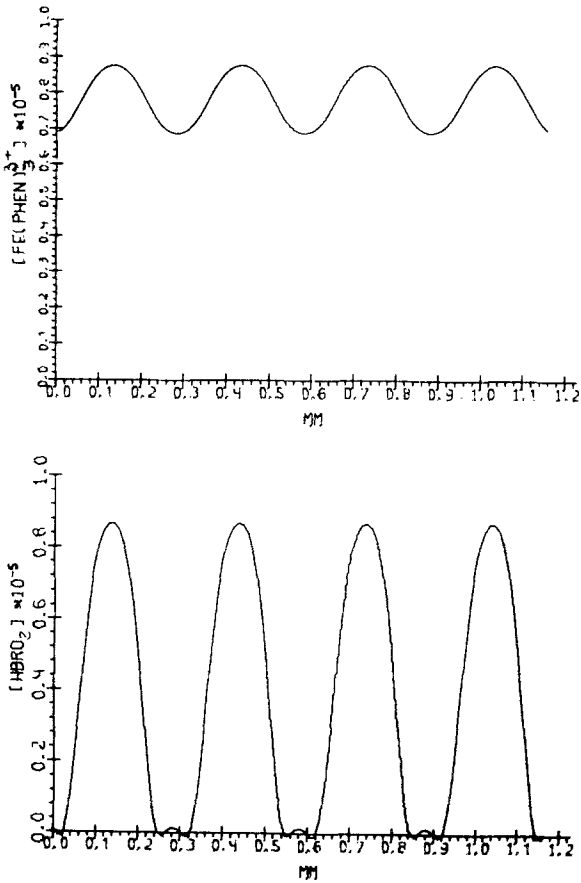

Fig. 7. Stationary periodic pattern of large amplitude for $A = 0.02$, $B = 0.192$, $C = 10^{-5}$, $h_0 = 1$, $\kappa = 25$.

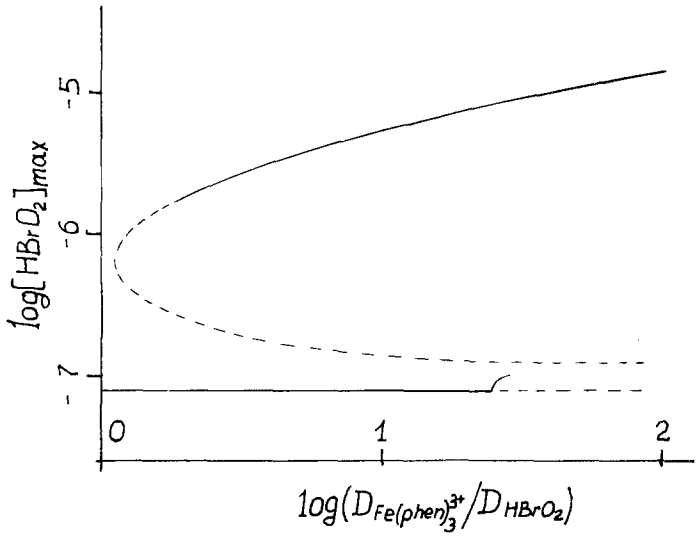

Fig. 8. Stationary state diagram for $A = 0.02$, $B = 0.192$, $C = 10^{-5}$, $h_0 = 1$.

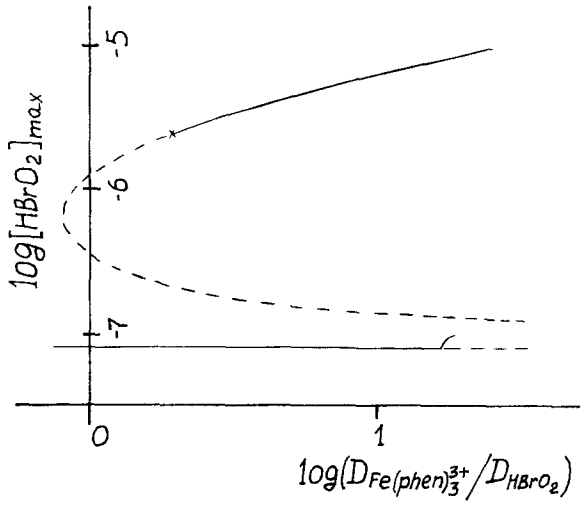

Fig. 9. Stationary state diagram for $C = 1.8 \times 10^{-5}$. Other values as for Fig. 8.

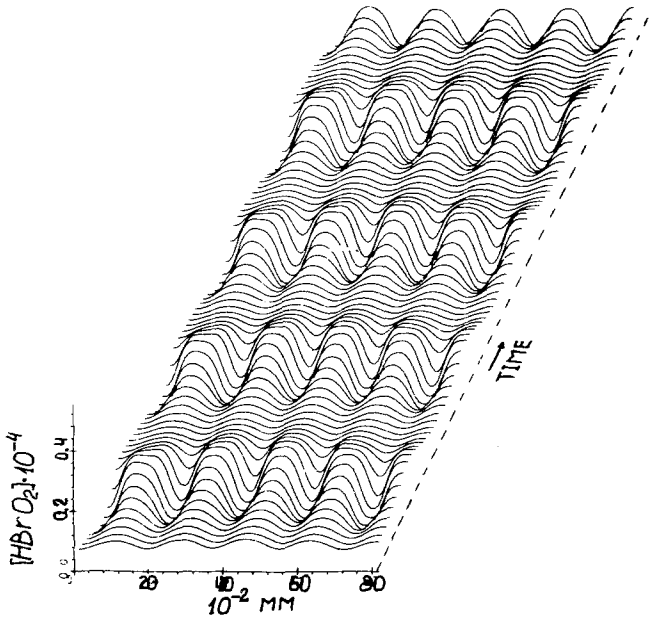

Fig. 10. Nonlinear standing wave for $A = 0.1$, $B = 0.15$, $C = 3 \times 10^{-4}$, $h_0 = 0.5$, $\kappa = 2$. Time interval between adjacent profiles is 0.5 sec.

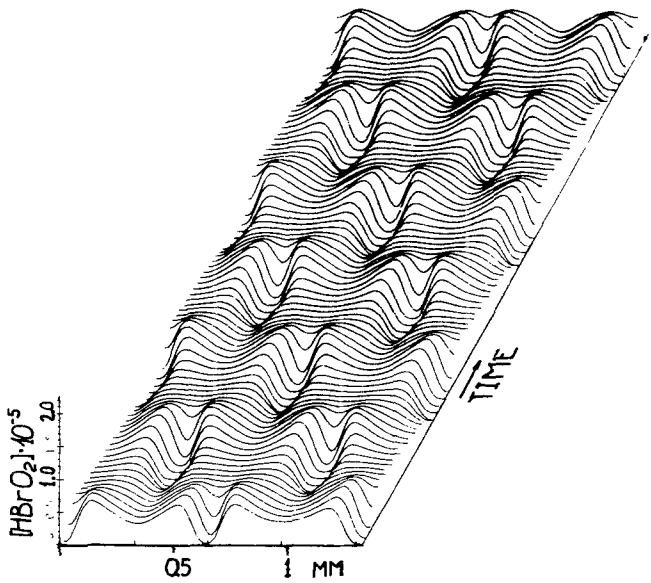

Fig. 11. Nonlinear standing wave for $A = 0.04$, $B = 0.01$, $C = 3 \times 10^{-4}$, $h_0 = 0.5$, $\kappa = 1.7$. Time interval between adjacent profiles is 1 sec.

shows the bifurcation diagram for this case. The solid lines correspond to the stable solutions and the dashed lines correspond to the unstable solutions. The interval $2.7 < \kappa < 20$ is a bistability region where both the homogeneous state and the large-amplitude stationary pattern are stable. Figure 9 shows that a large-amplitude stationary structure can also exist for $\kappa < 1$. However, in the case presented it is unstable. The asterisk marks the point where stability is lost. Such an instability can lead to the appearance of standing waves.

Examples of standing waves are given in Figs. 10 and 11. The period of temporal oscillations of the standing wave rises with diminishing κ and goes to infinity when $\kappa \to \kappa_2$. Such behavior usually means that some analog of a homoclinic orbit exists in the system (17) at κ_2. Shilnikov[23–25] has shown that bifurcations of homoclinic orbit can give rise to multiperiodic and irregular oscillations. Indeed, under certain conditions chaotic oscillations are observed in the system for κ close to κ_2 (Fig. 12). Figure 13 shows the projection of the oscillations onto the plane (x_1, x_2), where x_1 is $[HBrO_2]$ at the left reactor wall and x_2 is $[HBrO_2]$ at the right one. Next maximum and next minimum maps are given in Fig. 14. Figure 15 presents another chaotic pattern.

To provide a deeper insight into a mechanism of standing waves

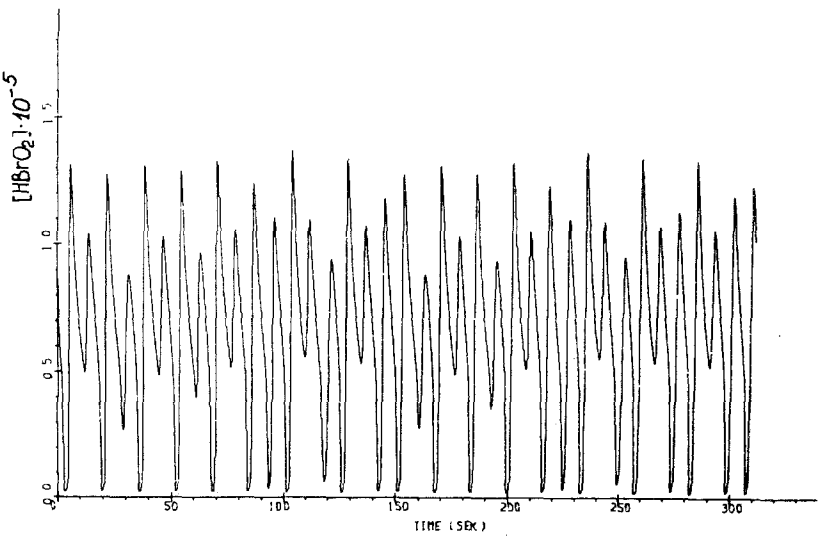

Fig. 12. Chaotic oscillations at the left wall of the reactor. $A = 0.0972$, $B = 0.15$, $C = 3 \times 10^{-4}$, $h_0 = 0.5$, $\kappa = 1.632$.

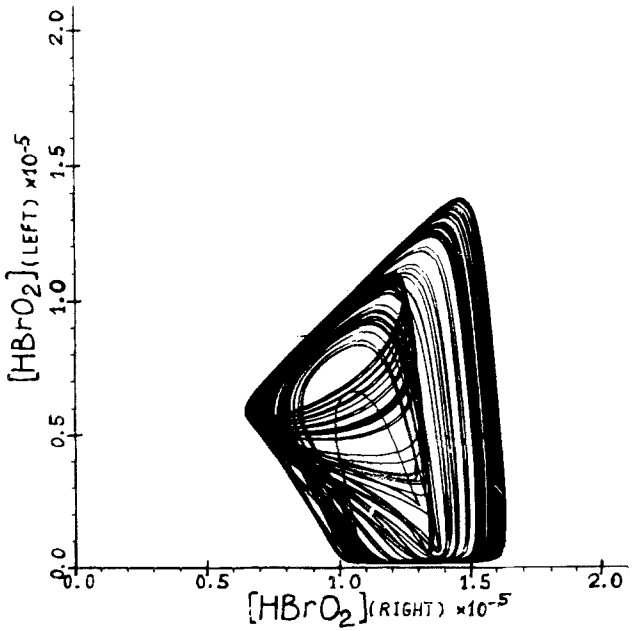

Fig. 13. Two-dimensional projection of the attractor for the motion illustrated by Fig. 12.

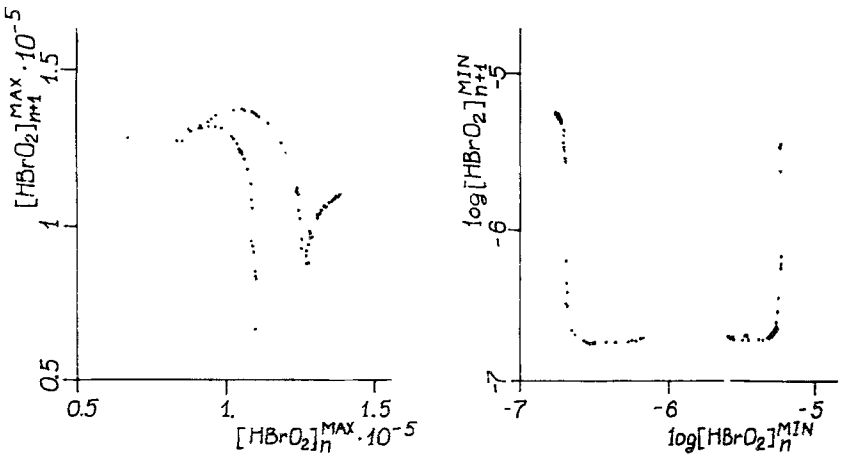

Fig. 14. Next maximum and next minimum maps for the regime show in Fig. 12 (for the first 80 peaks).

and chaotic oscillations, one may consider the ODE system that is a discretization of the PDE system (17):

$$\frac{dx_i}{d\tau} = \frac{1}{\varepsilon} f(x_i, z_i) + \frac{1}{h^2}(x_{i-1} + x_{i+1} - 2x_i)$$
$$\frac{\partial z_i}{\partial \tau} = g(x_i, z_i) + \frac{\kappa}{h^2}(z_i + z_{i+1} - 2z_i) \tag{18}$$

where h is a space interval between two neighboring mesh points. Stationary solutions of system (18) were followed with a Newtonian iteration technique and the eigenvalues of the stationary states were calculated with the QR method. The stationary state diagram with bifurcation points and oscillation region (κ_2, κ_1) is given in Fig. 16. The point κ_1 is a point of Hopf bifurcation in the system (17), (18). As a result of the bifurcation the large-amplitude stationary periodic patern loses its stability and a standing wave with the same spatial period appears. When κ

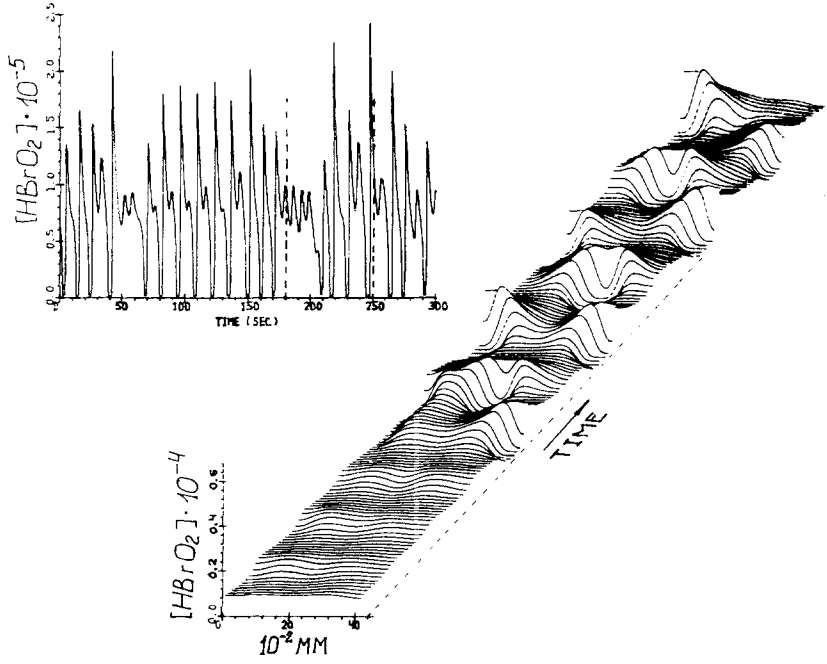

Fig. 15. Spatiotemporal structure for $A = 0.0965$, $B = 0.15$, $C = 3 \times 10^{-4}$, $h_0 = 0.5$, $\kappa = 1.6$. Top left: $[HBrO_2]$ oscillations at the left end of the reactor. Vertical dashed lines bound the time interval for which the structure on the main figure is shown. Time interval between two adjacent profiles of the structure is 0.5 sec.

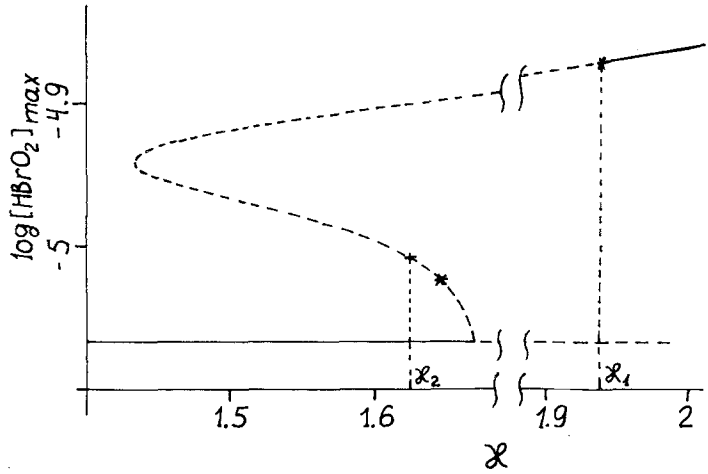

Fig. 16. Steady-state bifurcation diagram for $A = 0.0972$, $B = 0.15$, $C = 3 \times 10^{-4}$, $h_0 = 0.5$. A saddle point with the saddle number $S_1 = 0$ is indicated by the asterisk. To the left of the asterisk the saddle points have positive S_1.

diminishes, the temporal period rises and goes to infinity. At κ_2 the limit cycle corresponding to the standing wave becomes a homoclinic orbit which goes from and returns to the saddle-focus stationary state marked in Fig. 16 with an asterisk.

The bifurcation of a homoclinic orbit was studied in detail by Shilnikov.[23 25] He showed that its character strongly depends on saddle numbers. Let a saddle-focus have a single real, positive eigenvalue and a

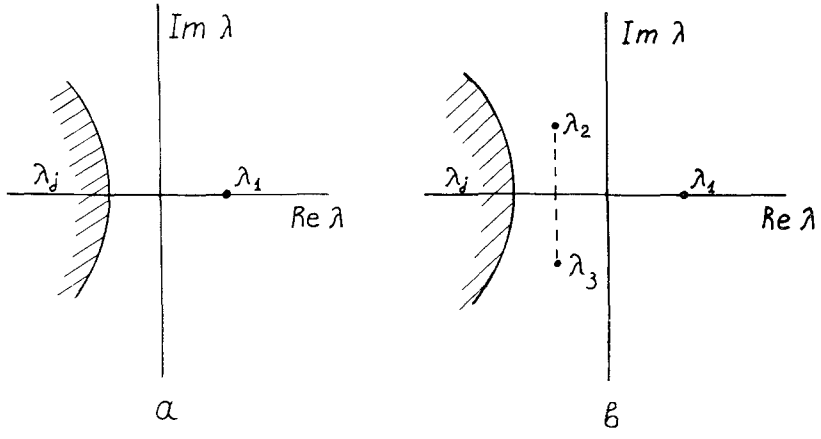

Fig. 17. Eigenvalues of an ODE system on the complex plane.

conjugate complex pair of eigenvalues closest to the imaginary axes in the left semiplane (Fig. 17). The saddle numbers are determined by the following expressions:

$$S_1 = \mathrm{Re}\,\lambda_{2,3} + \lambda_1, \qquad S_2 = 2\,\mathrm{Re}\,\lambda_{2,3} + \lambda_1$$

If $S_1 < 0$, then a limit cycle bifurcates, but if $S_1 > 0$, the bifurcation is more complex. If at the same time $S_2 < 0$, then in the vicinity of the bifurcation point in the parameter space an infinite sequence of multiperiodic motions exist, which are conected with period-doubling bifurcations. If $S_2 > 0$, then the motion is quite unstable.

4. CONCLUSION

Thus, we have presented a model of the ferroin-catalyzed BZ reaction which quantitatively describes most of the experimental results. This model can be used to predict new effects and dynamic regimes. In particular, this model predicts that in the system, the interaction of reaction and diffusion can break the stability of the steady state and then stationary periodic structures, nonlinear standing waves, or chaotic spatiotemporal structures of large amplitude can appear in the system. One hopes that it will be possible to find a way of experimentally realizing these regimes.

REFERENCES

1. I. Prigogine, *Introduction to Thermodynamics of Irreversible Process* (Thomas, Springfield, Illinois, 1955).
2. P. Glansdorf and I. Prigogine, *Thermodynamic Theory of Structure, Stability and Fluctuations* (Wiley-Interscience, 1971).
3. B. P. Belouson, *Zb. Ref. Rad. Med.* **1958**:145.
4. A. M. Zhabotinsky, *Dokl. Akad. Nauk SSSR* **157**:392 (1964).
5. A. N. Zaikin and A. M. Zhabotinsky, *Nature* **225**:535 (1970).
6. A. M. Zhabotinsky and A. N. Zaikin, *Oscillatory Processes in Biological and Chemical Systems* (Puschino, 1971), p. 279 (in Russian).
7. A. T. Winfree, *Science* **175**:634 (1972).
8. R. J. Field, EE. Körös, and R. M. Noyes, *J. Am. Chem. Soc.* **94**:8649 (1972).
9. A. B. Rovinsky and A. M. Zhabotinsky, *Teor. Eksp. Khim.* **14**:182 (1978).
10. A. B. Rovinsky and A. M. Zhabotinsky, *Teor. Eksp. Khim.* **15**:25 (1979).
11. Z. Noszticius, H. Farkas, and Z. Shelly, *J. Chem. Phys.* **80**:6062 (1984).
12. L. Kuhnert, H.-J. Krug, and L. Pohlmann, *J. Phys. Chem.* **89**:2022 (1985).
13. A. B. Rovinsky and A. M. Zhabotinsky, *J. Phys. Chem.* **88**:6081 (1984).
14. A. B. Rovinsky, *J. Phys. Chem.* **90**:217 (1986).
15. A. Turing, *Phil. Trans. R. Soc.* **237B**:37 (1952).
16. A. B. Rovinsky and A. M. Zhabotinsky, in *Fundamental Research in Chemical Kinetics*, A. E. Shilov, ed. (Gordon and Breach, 1986).

17. A. B. Rovinsky, *J. Phys. Chem.* **88**:4 (1984).
18. F. Ariese and Z. Nagi-Ungvarai, *J. Phys. Chem.* **90**:1 (1986).
19. F. Ariese and Z. Nagi-Ungvarai, *J. Phys. Chem.* **90**:1496 (1986).
20. R. J. Field and H.-D. Försterling, *J. Phys. Chem.* **90**:5400 (1986).
21. G. Ioss and D. Joseph, *Elementary Stability and Bifurcation Theory* (Springer-Verlag, 1980).
22. B. D. Hassard, P. D. Kazarinoff, and J.-H. Wan, *Theory and Application of Hopf Bifurcation* (Cambridge University Press, 1981).
23. L. P. Shilnikov, *Matem. Zb.* **61**:104, 433 (1963).
24. L. P. Shilnikov, *Dokl. Akad. Nauk USSR* **170**:49 (196).
25. L. P. Shilnikov, *Matem. Zb.* 77:461 (1968).